ISSN: 0067-2904

Hybrid Techniques with Support Vector Machine for Improving Artifact Ultrasound Images

Ayat Ali Al-Jaburi*, Ahlam Hanoon Al-Sudani
Computer Eng. Department, College of Engineering, University of Baghdad, Baghdad, Iraq

Received: 19/1/2022 Accepted: 21/6/2022 Published: 28/2/2023

Abstract

The most common artifacts in ultrasound (US) imaging are reverberation and comet-tail. These are multiple reflection echoing the interface that causing them, and result in ghost echoes in the ultrasound image. A method to reduce these unwanted artifacts using a Otsu thresholding to find region of interest (reflection echoes) and output applied to median filter to remove noise. The developed method significantly reduced the magnitude of the reverberation and comet-tail artifacts. Support Vector Machine (SVM) algorithm is most suitable for hyperplane differentiate. For that, we use image enhancement, extraction of feature, region of interest, Otsu thresholding, and finally classification image datasets to normal or abnormal image. Because of the machine's training for both types of images, the machine can now predict whether a new image is an abnormal image or a normal image. As a result, it reduced medical work for many checkups and other things. Our proposed method shows the correct classification result by more than 89%.

Keywords: Comet-tail artifact**,** Reverberation artifact, Support vector machine, Otsu thresholding, Artifacts.

تحسين صور الموجات فوق الصوتية (السونار) المتضررة باستخدام تقنيات متعددة مع Support Vector Machine

آيات علي الجبوري *,احلام حنون السوداني
كلية الهندسة، قسم هندسة الحاسبات، جامعة بغداد، بغداد، العراق

الخلاصة

أكثر Artifacts شيوعًا في جهاز السونار الطبي هي الصدى وذيل المذنب. هذه انعكاسات متعددة أصداء الواجهة التي تسببها ، وتؤدي إلى أصداء شبحية في صورة جهاز السونار الطبي . طريقة لتقليل هذه Artifactsغير المرغوب فيها باستعمال عتبة Otsu للعثور على منطقة الاهتمام (أصداء الانعكاس) والإخراج المطبق على مرشح متوسط لإزالة الضوضاء. الطريقة التي تم تطويرها قللت بشكل كبير من حجم الآثار الصدى وذيل المذنب. أفضل خوارزمية Support vector machine للتمايز المفرط. لذلك نستخدم تحسين الصورة ، واستخراج الميزات ، والعثور على المنطقة ذات الأهمية باستخدام عتبة Otsu ، وأخيراً نصنف مجموعة بيانات الصورة بالصورة العادية أو الصورة غير الطبيعية. بسبب تدريب الآلة لكل من نوع الصورة ،

*Email: ayata8179@gmail.com

ستتمكن الآلة الآن من التنبؤ بالصورة الجديدة حيث توجد صورة غير طبيعية أو صورة عادية. لذلك ، قلل من العمل الطبي للعديد من الفحوصات والجميع. مع طريقتنا المقترحة أكثر من 89٪ نجد نتيجة التصنيف الصحيحة.

1. Introduction

The optical microscope was historically the first medical imaging machine to be used, followed by x-rays that began in the 19th century and US imaging in the middle of the 20th. Subsequently, 3D imaging techniques such as Computed Tomography (CT) and Magnetic Resonance Imaging (MRI)[1]. Ultrasound medical imaging, due to its many advantages, is one of the most commonly applied methods today. It consists of a mechanical length wave using a frequency that exceeds the top limits of the human auditory system[2]. The benefits of ultrasound include safety, low cost, non-invasiveness, and in-pocket portability which have made it an advantageous tool for showing accurate information about medical soft tissue[3].

Medical images contain vital information that clinicians require in order to diagnose and treat patients. The diagnostic process heavily relies on image visual perception. Unfortunately, the possibility of perception error and quality of low image are barriers to effective extraction of features, analysis, recognition, and quantitative of measurements which are not acceptable because it primarily affects the patients' lives. Image enhancement improves image visual quality, assists clinicians in making decisions, and thus saves patients' lives[4].

In the medical field, ultrasound imaging is widely used. Soft tissues in organs such as liver, kidney, spleen, uterus, heart, and brain, among others, are imaged using it. Speckle noise is the most common problem in ultrasound images, and it is caused by the imaging technique used, which can range from acoustic to laser imaging[5],[6].

There have been numerous works on the enhancement of images that have been tainted by noise. To remove noise from an image, a variety of filters are used by determining a more accurate version from pixels. Extremely "noisy" pixels can be filtered out by taking into account neighboring pixels. Regrettably, extreme pixels can represent genuine fine details that are lost during the smoothing process. There is no one-of-a-kind method for removing noise from an image that has been affected. Depending on the noise model, various algorithms are employed. Because of its excellent de-noising power capability[7] and computational efficiency[8], the median filter was once the most popular nonlinear filter for noise removal.

Although the technological progress on the diagnostic ultrasound of equipment is very important, artifacts remain the diagnostic challenge for the radiologist. Artifacts may be described as seen in the images' echoes that do not reflect the real picture of patients in their intensity or location[9]. These artifacts have an effect on image quality. We have classified it into three groups: artifacts caused by the patient, artifact caused by instruments, and artifact caused by the operator (technique artifact). Segmentation is the process of making a picture more understandable and easier to analyze by simplifying and/or modifying its representation[10]. The technique of image segmentation is widely used to detect objects and edges in images. For identifying the area of interest under examination, medical picture segmentation is required. Almost all medical situations require it[10].

The proposed method of classification consist of a training set, feature extraction using principal component analysis (PCA), classifier using SVM, and testing set. The suggested method differs from earlier work in that it employs several kernels to improve performance

and examine parameter optimal values. Linear, polynomial, radial basis function (RBF), and sigmoid are the four most used kernel functions. Additionally, the contribution of this paper is high accuracy of classification by using 257 images. The accuracy of classification reach to 89%.

2. Literature Review

In recent years, researchers have achieved many successes in improving the image classification, which is closer to the livelihood of people in medicine. Currently, some people have achieved good image quality improvement results.

Vanitha L. and Venmathi A. R [11] proposed work, the features of the bacterial image are extracted and SVM is used for classifying the bacterial types. SVM have high approximation capability and much faster convergence.

Sudhamshu Mohan S. et al. [12] as a preliminary step, here is an attempt to design an autonomous system which is based on SVM Classifier in which noise is classified into different types so that each type can be dealt in an optimal way. This work will address the challenge of characterizing noise and deciding the extent of de-noising, there by caters the physician in subsequent analysis.

Jyoti Verma et al.[13] as project, is based on multiclass problem according to this research these techniques should not be the only method to solve these practical problems. For that we use image enhancement, morphological operation, feature extraction, region of interest using segmentation techniques and finally classify the image dataset with kidney stone detection or without stone. Because of training of the machine for both the type of image, now machine will able to predict the new kidney image that whether it is an abnormal kidney image that has stone or normal kidney image having no stone. Therefore, it reduces medical work for many checkup and all. Proposed algorithm more than 85% we find correct classification result.
Abbas et al. [14] extracted ten different Gray-Level Co-occurrence Matrix (GLCM) features of a segmented skin lesion and performed classification using SVM. The performance of the classifier is evaluated based on sensitivity, accuracy and specificity. Öztürk et al. [15] extracted features of histopathologic images for identifying the cancerous regions by applying GLCM, Local Binary Pat- terns (LBP) and other feature extraction methods. KNN, SVM and Boosted Trees classifier are used for classification of these images.

S. Vani Kumari and K. Usha Rani [16], the aim of this work is to find the feature extraction method that is best for classifying the medical images. Local Binary Patterns (LBP), Gray-Level-Run-Length-Matrix (GLRM), Completed Local Binary Patterns (CLBP), GLCM and Local Tetra Patterns (LTrP) are the most prominent feature extraction methods for medical images and are considered in this study. Two well-known classifiers Multi-Layer Perceptron using Backpropagation Network (MLPBPN) and SVM are used to analyze the efficiency of above specified five feature extraction techniques. Five different medical image datasets are considered for experimentation. The experimental results illustrate that GLCM method is the best method compared with the other four feature extraction methods for medical image classification.

3. Ultrasound Image Artifacts

The US artifacts are any alterations in the image which do not represent an actual image of the examined area images so that the images that are seen but not present tissue structures or structures with incorrect locations and sizes such that the artifacts can affect the ability to

use US accurately. There are several types of artifacts that can be seen in B-mode US image, some of them are explained below:

- Reverberation artifact: It arises when there is a back and forth reflection for the US energy between two interfaces throughout the acquisition of the signal and prior to the following transmitted pulse[17]. As shown in Figure 1, the reverberation artifact in the anterior portion of the urinary bladder (red arrow).

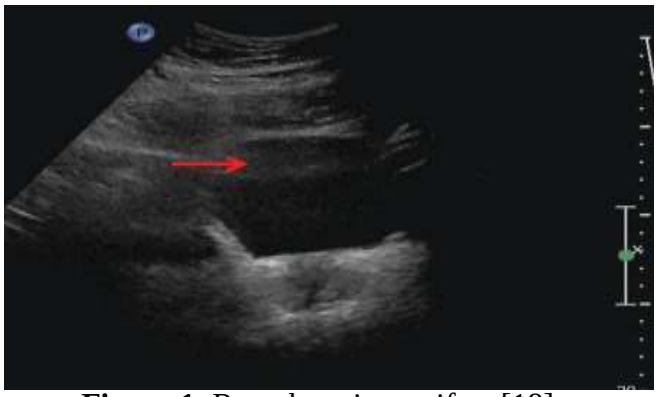

Figure 1: Reverberation artifact [18]

- Comet-tail: Is a type of the reverberation artifact, seems as dense tapering trail of echoes just distal to a robustly reflecting structure[19] as shown in Figure 2.

Figure 2: Comet-tail artifact [17]

- Side lobes: are secondary echoes that occur outside of the main beam. These echoes are erroneously positioned in the image, as though they came from the original packet. Side lobes can be reduced or removed by lowering the gain or changing the depth of the ultrasonic beam [20] as shown in Figure 3.

Figure 3- Side lobe artifacts [20]

- Time Gain Compensate: Extra echoes or insufficient echoes may be introduced as a result of inappropriate TGC utilization. Incorrect transducer selection can also result in a focus zone and frequency concentration on superficial structures. Excess gain can also cause (noise artifact) when a typically echo-free structure includes low-level noise[9] as shown in Figure 4.

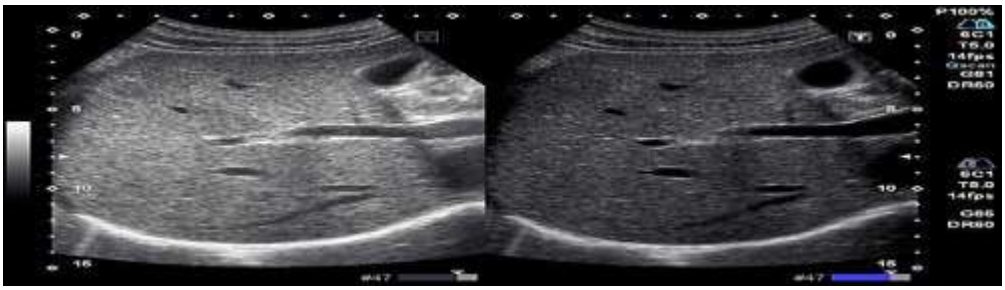

(a) (b)

Figure 4: Time Gain Compensate (TCG), (a) Focus too high (b) Focus low [9]

4. Materials and Procedures

Collecting of 2D ultrasound images, processing of distinct images using Otsu thresholding and median filter techniques, usage of the SVM algorithm, and examination of the output image using various parameter performance are all part of this experiment.

4.1 Image Processing Algorithms

Proposed methodology involves several steps such as Otsu thresholding to find region of interest. Removal of speckle noise using median filter and SVM of preprocessed images applied to predict normal image or abnormal image. The methodology is shown in Figure 5(a) and (b).

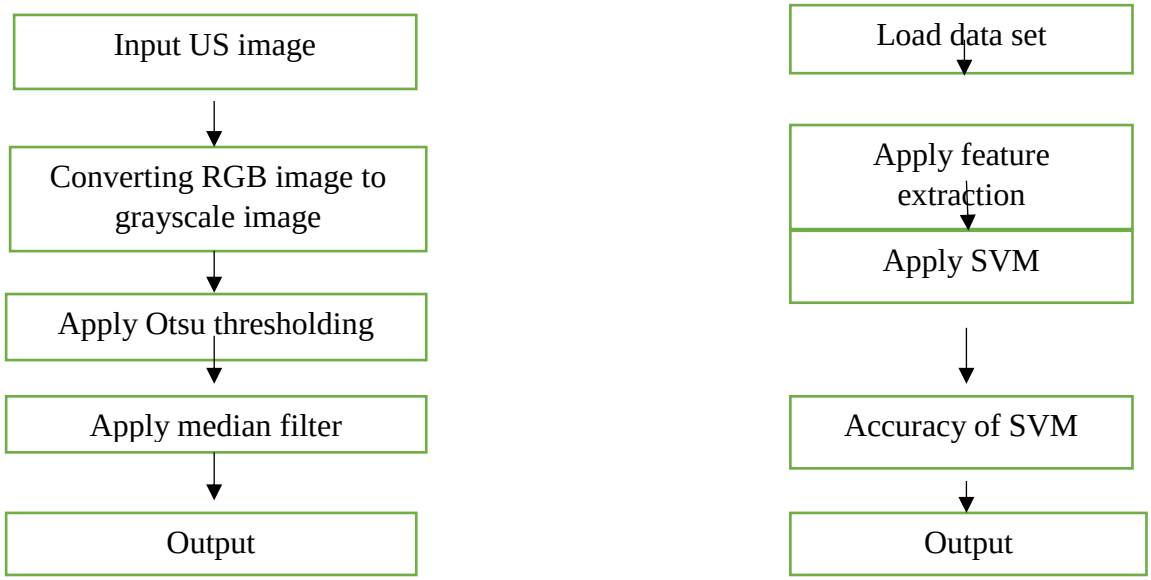

(a) (b)

Figure 5: Flowchart of the proposed methods, (a) Proposed method of reverberation and comet-tail artifact (b) Proposed method of the SVM

4.2 Otsu thresholding

In Otsu's method for determining a threshold, interclass variance is employed as a statistic. The best threshold values maximizes interclass variance. Let be $f(x, y)$ a grayscale image with pixel grey values ranging from 0 to $L-1$, where L is number of distinct grey levels. The total number of pixels that have the same grey level i is denoted by n_i. Then as Eq. (1)[21]:

$$N = \sum_{i=0}^{L-1} ni \tag{1}$$

The total number of pixels in the entire image.

In practice, if p_i represents the probability of a pixel which Grey level value i it can be approximated using frequency defined as $p_i = \frac{n_i}{N}$. If we use T as a value of threshold, the pixels in the image can then be divided into two classes for a binary segmentation task as C_0 and C_1. Where C_0 and $C_1$are pixel sets that contain pixels with greyscale the values are in the ranges [0, T] and [T + 1, L – 1], respectively. There are a few things to consider before delving into the definition of interclass variance a few key statistics to consider. These are as follows: the average pixel grey value of C_0 and C_1, as well as the weights parameters denoted by the symbols $\mu_0(T), \mu_1(T), \omega_0(t)$as well as $\omega_1(T)$. The statistics mentioned above can be defined as Eq. (2), (3) and (4)[21]:

$$\mu_0(T) = \frac{\sum_{i=0}^{T} ip_i}{\omega_0(T)} \quad , \omega_0(T) = \sum_{i=0}^{T} p_i \tag{2}$$

$$\mu_1(T) = \frac{\sum_{i=T+1}^{L} ip_i}{\omega_1(T)}, \omega_1(T) = \sum_{i=T+1}^{L} p_i \tag{3}$$

$$\mu = \frac{\sum_{i=0}^{L} ip_i}{\sum_{i=0}^{L} p_i} = \sum_{i=0}^{L} ip_i = \omega_0(T) \cdot \mu_0(T) + \omega_1(T) \cdot \mu_1(T) \tag{4}$$

In Eqs. (2) to (4), μ0(T) and μ1(T) are the ambiguous value assumptions of C_0, C_1, and μ represents the average grey value of all pixels in the entire image. According to the preceding definitions, the interclass variance of C_0, C_1 can be defined as $\sigma_B(T)$, where T represents a threshold value for segmentation, and $\sigma_B(T)$ is then defined in Eq.(5)[21]:

$$\sigma_B(T) = \omega_0(T)(\mu_0(T) - \mu)^2 + \omega_1(T)(\mu_1(T) - \mu)^2 \tag{5}$$

The variance of interclass in Eq. (5) consists of two parts, with the two terms representing the two classes C_0, $C_1$with different weights $\omega_0(T)$ and $\omega_1(T)$ which are defined in Eqs. (2) and (3). As previously stated, Otsu's algorithm takes into account the grey value T* as the optimal threshold if the interclass variance $\sigma_B(T)$ ofC_0, C_1 reaches its maxmium value when using T* as the threshold value. The optimal value of threshold T* can be showed as solving an optimisation problem as shown in Eq. (6)[21]:

$$T^* = argmax_T(\sigma_B(T)) \tag{6}$$

4.3 Median Filter

Median filtering is a nonlinear method for eliminating noise from photographs. It is popular since it is good at reducing noise while maintaining sharp edges. It is extremely effective at removing "salt and pepper" sounds. The median filter replaces each value with the median of nearby pixels as it traverses the image pixel by pixel. The "window" is a pattern of neighbors that moves pixel by pixel over the entire image. As illustrated in Figure 6, the median is derived by numerically sorting all of the pixel values in the window and then replacing the pixel in question with the middle (median) pixel value. Because it keeps certain useful features in an image, median filtering is preferable than mean filtering[22].

123	125	126	130	140
122	124	126	127	135
118	120	150	125	134
119	115	119	123	133
111	116	110	120	130

Neighborhood of values: 115, 119, 123, 125, 127, 126, 124, 120, 150

Median value: 124

Figure 6: Calculating a pixel neighborhood's median value[22]

4.4 Support Vector Machine

Vapnik et al.[23],[24] created SVM, a well-known supervised machine learning approach. It is also utilized to perform categorization tasks. The data is frequently divided into training and testing sets because each case comprises several qualities (features) and labels (target values). This model will only be used to predict test labels based on the data collected during the testing features[23]. The goal of SVM is to generate a decision surface by constructing a separating hyperplane with the greatest possible margin between the positive and negative outcomes. For lower generalization error, larger margins are require[25]. It is worth mentioning that, all the kernel parameters, support vector, y_i , a , b and label names are stored in the prediction model. In addition, the kernel function, is used to achieve better performance and analyze the optimal values of the parameters. Four types of kernel functions are commonly used which are: linear, polynomial, Radial Basis Function (RBF) and sigmoid. For each kernel, several parameters are need to be tuned[23]. Because it gives a non-linear mapping, the RBF is a good first choice. This mapping to a higher dimensional space will provide an appropriate solution especially when the labels and attributes are non-linearly related. Furthermore, by minimizing the number of created hyperplanes, it reduces the complexity. The RBF can be expressed as Eq. (7)[23].

$$K(x_i, x_j) = \exp(-g\|x_i - x_j\|^2 + C) \quad (7)$$

Where g (gamma) is the parameter of the kernel and C is the cost parameter of SVM. To tune the SVM parameters, the cross validation is implemented to select the optimal values and provide an accurate predication[23].

4.5 Variable definition to build SVM

1. Let x indicate an input space drawn vector, presumed m_o-dimensional.
2. Let { φ_j (x)} for j=1 to m_1, indicate a set of nonlinear input space transformations to the function space.
3. m_1 is the space characteristic dimension.
4. {w_j} for j=1 to m_1 refers to a set of linear weights that link the space with the output.
5. {φ_j (x)} is the input that the weight w_j is supplied through the functional space.
6. b is the bias.
7.α_i the coefficient of Lagrange.
8. d_i matching output target.

Steps to build SVM:

a. Hyperplanes acting as the surface of decision as Eq. (8)[12]:

$$\sum_{i=1}^{N} a_i d_i K(x_1\, x_i) = 0 \tag{8}$$

Where

$K(X, X_i) = \varphi^T(X)\varphi(X_i)$ Represents two vectors induced by the input within the function space vector x and input pattern xi for example. This term is called the kernel of the internal product in Eq. (9), (10) and (11)[12]:

Where

$$w = \sum_{i=1}^{N} a_i d_i \varphi(x_i) \tag{9}$$

$$\varphi(x) = [\varphi_0(X), \varphi_1(X), \dots, \varphi_{m1}(X)]^T \tag{10}$$

$$\varphi_0(X) = 1\ for\ all\ X \tag{11}$$

w_0 Denotes the bias b.

b. Mercer's theorem must be fulfilled for the K (x, xi) kernel. The function kernel was selected as a learning polynomial in Eq. (12)[12]:

$$K(X, X_i) = (1 + X^T X_i)^2 \tag{12}$$

c. $\{\alpha_i\}$ Lagrange multiplier for i = 1 to N maximizing Q (α), as 0, i is referred to as $\alpha_{0,i}$determined in Eq. (13)[12].

$$Q(\alpha) \sum_{i=1}^{N} = \alpha_i - \frac{1}{2}\sum_{i=1}^{N}\ \sum_{j=1}^{N} \alpha_i \alpha_j d_i d_j K(X_i, X_j) \tag{13}$$

Subject to the following restrictions in Eq. (14)[12]:

$$\sum_{i=i}^{N} a_i d_i = 0 \tag{14}$$

$0 \le \alpha_i \le C$ for i=1, 2,…, N

d. Using the following formula, the linear weight vector W_0, which corresponds to Lagrange Multiplier optimum values, in Eq. (15)[12]:

$$w_0 \sum_{i=1}^{N} \alpha_{0,i} d_i \varphi(x_i) \tag{15}$$

$\varphi(X_i)$Is a feature space induced image byX_i.

W_0 is the optimal biological bias b_0.

e. And the decision function is defined in Eq. (16)[23]:

$$sgn(w^T \emptyset(x_i) + b) = sgn(\sum_{i=0}^{n} y_i a_i K(x_i, x_j) + b) \tag{16}$$

Where sgn is the signum function and defined in Eq. (17)[23]:

$$sgn(x) = \begin{cases} -1 & if\ x < 0 \\ 0 & if\ x = 0 \\ 1 & if\ x > 0 \end{cases} \tag{17}$$

5. The Proposed Method for Reducing Reverberation and Comet-tail Artifacts

The image of the US is an RGB image. This image has been converted to a grayscale. This image is affected by a variety of noises, including speckle noise and artifacts. We process this image in Python because of the open-source python libraries in image processing tasks. It offers features that other libraries do not, such as filtering, opening manipulating and saving images. Steps of the proposed method are described in more details in Algorithm (1).

Algorithm (1): The proposed method of reducing US artifacts.

Step 1: US input image.

InputImg = cv2.imread (Input).

Step 2: Converting RGB image to the grayscale image.

InputImg = cv2.cvtColor (InputImg, cv2.COLOR_BGR2GRAY).

Step 3: Applying Otsu thresholding method to the step 2.

cv2.threshold

Step 4: Applying median filter to the step 3.

Median = cv2.medianBlur (InputImg, kernel size)

Output: Despeckling image.

6. The Proposed Classification Algorithm

For classification, the suggested method employs the SVM, a supervised machine learning algorithm. SVM classifiers have a wide range of applications. SVM maximizes the distance between the separating hyperplane and the data, for starters. As a result, SVM decreases structural risk by limiting out-of-sample error. By constructing a hyperplane, SVM can distinguish between positive and negative image[26].

Second, SVM is well-suited to classification problems and has a high level of noise resistance[26]. To distinguish between normal and abnormal images is illustrated in Figure 7:

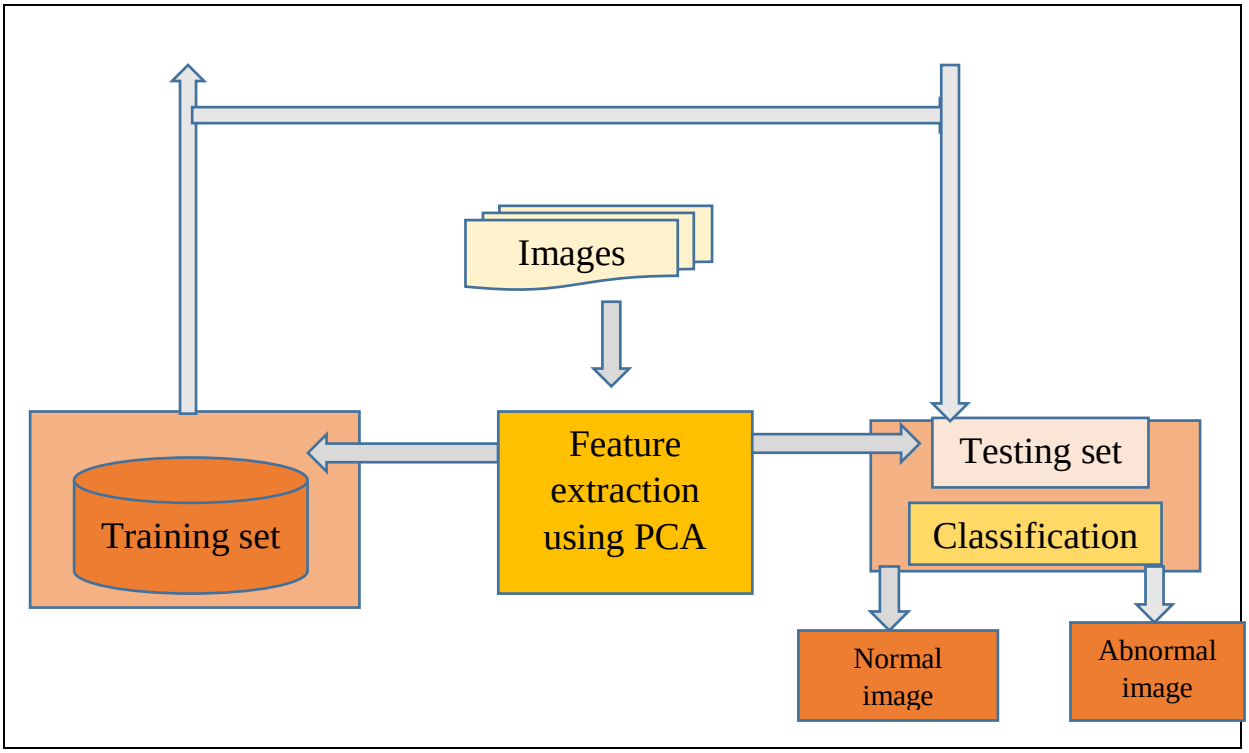

Figure 7: Proposed method of SVM

As the above figure depicts that given image set is divided into training set, which is used to train the classifier and test set which is used to check the performance of the classifier. In this paper, 257 different images which was normal and abnormal are used for training classifier. Principal component analysis (PCA) is ultrasound data analyzing method which is used to compress high dimensional data vector sets into low dimensional ones and solve multiclass problems. PCA is derived from many starting points and optimization criteria in order to reduce the dimension of data, the most important data optimization is minimization of mean-square error in data which is compressed and PCA locates the mutual orthogonal point directions in given images dataset with max variances as observed by the PCA. This PCA features are used for training SVM classifier, which is a multiclass classifier. The approach employed in this work is basically one versus many approach, in which a decision is taken based on the decision a given test feature belongs to a particular class as SVM is basically a binary classifier Thus the output of this classifier is basically one of the following classes: 1) normal image 2) abnormal image.

7. Parameter Analysis

We can use several analysis performance parameters to analysis the result of segmentation technique. We used five metrics, namely dice coefficient (DC) [27], Jaccard Index[28], mean square error (MSE), peak to noise ratio and accuracy as analysis parameter.

❖ (DC): measures the similarity of two images. The resulting segmented image with the original image that marked by medical experts was compared with the dice coefficient. It is possible to calculate by Eq. (18)[29]:

$$DC=\frac{2.|B1\cap B2|}{|B1|+|B2|} \quad (18)$$

B1 represents a segmented image in Eq. (18). B2 is the original image before the processing.

❖ Jaccard Index.: the Jaccard index (JI) is used to identify similarities between two image samples. The ratio of size of the crossing to the union sample size is defined. The Jaccard index is similar also to the coefficient dice. It is between 0 and 1. The JI value is 1 for the exact same image and 0 for not same. The Eq. (19)[29]:

$$JI=\frac{|B1\cap B2|}{|B1\cup B2|} \quad (19)$$

B1 represents a segmented image in Eq. (19).B2 is the original image before the processing

❖ The MSE discrepancy between the filtered and original images. MSE is a metric that may be used to quantify the difference between the values implied by an estimate and the genuine quality being certified in a number of methods. Eq. (20) is used to calculate MSE, where M and N are the image width and height, enhanced image B (i, j), and original image A (i , j). The i and j in the original and enhanced images, respectively, represent the row and column pixels[30].

$$MSE = \frac{1}{M*N}\sum_{i=0,j=0}^{M-1,N-1}[B(i,j) - A(i,j]^2 \quad (20)$$

❖ The Peak Signal to Noise Ratio is the ratio of maximum possible power to corrupting noise that affects image representation. In other words, PSNR is an engineering term for the ratio between the maximum possible power of a signal and the power of corrupting noise that affects the fidelity of its representation. PSNR is commonly expressed on a decibel scale. The PSNR is commonly used as a measure of image reconstruction quality, as shown in Eq. (21)[30].

$$PSNR = 20log_{10}\left[\frac{(2^n-1)}{\sqrt{MSE}}\right][dB] \quad (21)$$

❖ Accuracy: The classification process accuracy is determined by correct and incorrect predictions. As in Eq. (22) is used to calculate the classification process accuracy[31].

$$\text{Accuracy} = \frac{Number\ of\ correctly\ classified\ images}{total\ number\ of\ images} \quad (22)$$

8. Implementation and Result

In this paper, the execution is done on Intel core i5 (PyCharm 2020.3.4) using Python version 3.8.6. To reduce these artifacts (reverberation artifact as shown in Figure 8 and comet-tail artifact as shown in Figure 9). We implemented a method by converting RGB image to grayscale image as shown in Figure 10(a) and (b). To find region of interest, we used Otsu thresholding (we test many values of Otsu thresholding and we found these images as shown in Figure 11(a) and (b) best visually). We analyzed these images by measuring DC, JI and calculated run time in second for this step. Table 1- illustrates values of DC, JI and run time in second. We can see the value of DC is one for both artifacts and value of JI is 0.001430 for reverberation artifact and 0.002865 for comet-tail artifact. We achieved a fast implementation in run time. To remove noise from images, we sent output images from Otsu thresholding to median filter. In Figure 12 (a) and (b) images after median filter. We can minimize MSE to reach zero with higher PSNR reach to 361. Table 2 shows values of MSE and PSNR (dB). The RBF kernel is regarded to be a good choice since it tackles the nonlinear link between class labels and attributes. To obtain excellent RBF kernel parameters for reliable testing data

prediction, the Cross-Validation (CV) approach is performed. Cost parameter (C) and Gamma (g), an RBF parameter, are SVM penalty parameters, must be tuned. The accuracy of the RBF kernel is 89%, Polynomial 86%, sigmoid 84% and linear 81%. These values of accuracy are shown in Table 3.

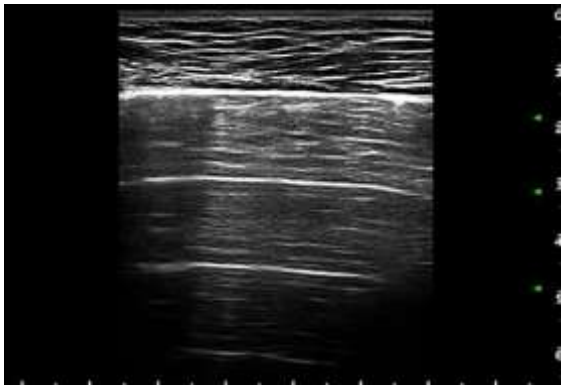

(a)

Figure 8: Reverberation artifact [9]

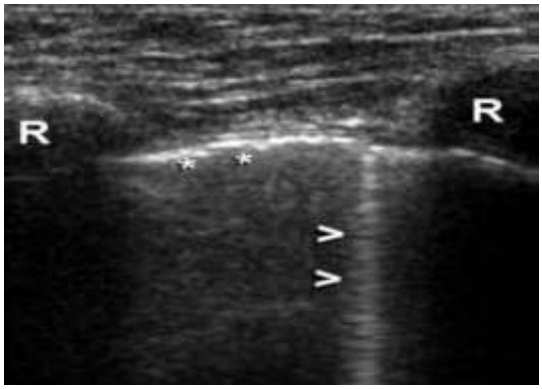

(b)

Figure 9: Comet-tail artifact [9]

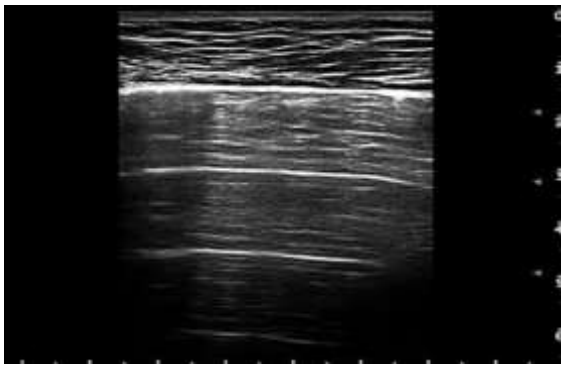

(a)

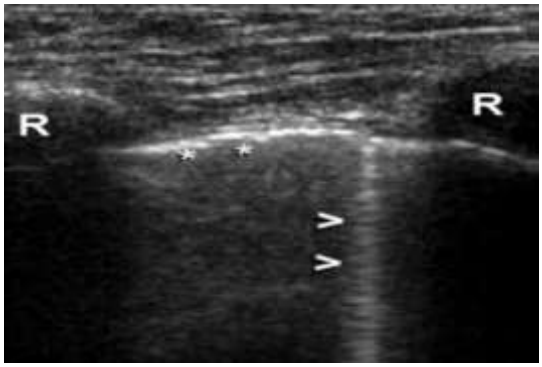

(b)

Figure 10: Gray images: (a) reverberation artifacts (b) comet-tail artifact

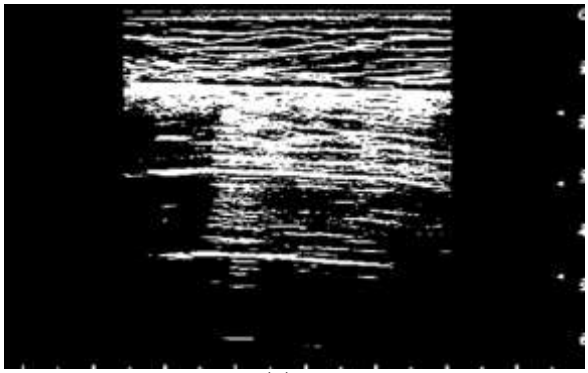

(a)

(b)

Figure 11: Thresholding images: (a) reverberation artifacts (b) comet-tail artifact

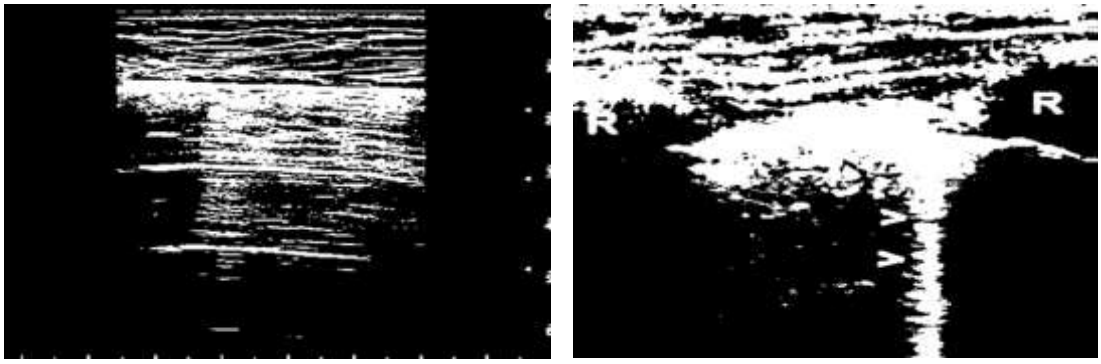

(a) (b)

Figure 12: Image after median filter: (a) reverberation artifacts (b) comet-tail artifact

Table 1: Values of DC, JI and run time for reverberation and comet-tail artifact

Type of artifact	DC	JI	Runtime (sec.)
Reverberation artifact	1.0	0.001430	0.11355
Comet-tail artifact	1.0	0.002865	0.08900

Table 2: Values of MSE and PSNR after median filter

Type of artifact	MSE	PSNR(dB)
Reverberation artifact	0.0	361.2019
Comet-tail artifact	0.0	361.2019

Table 3: Accuracy of trained models using different kernel function

Kernel function	Accuracy of trained model
RBF	89.23
Polynomial	86.15
sigmoid	84.61
Linear	81.53

9. Conclusions

We have tried to address the major problem in the processing of medical images in this paper: noise and artifacts medical images like magnetics, x-rays, ultrasound scans, etc., which are an important tools for diagnosing and researching various diseases. It is also important for these images to be as sharp as possible, given the increasing importance of their use. Nonetheless, in some cases all the help to interpret the images is needed. This paper focuses on ultrasound images and in particular on the method of eliminating the usual noisy and artifact images of this type: the so-called speckle noise, reverberation and comet-tail artifacts were examined that was based on Otsu thresholding to find region of interest and applied median filter to smooth image. As we showed in our method that we can minimize MSE to reach zero with higher PSNR reach to 361. The proposed method using SVM as a classifier for classification of medical US image provided a good classification efficiency of 89%. The proposed computational accuracy can be and yields a good result. By extracting more features and expanding the training set, classification accuracy can be improved.

Reference

[1] S. F. Keevil, "Physics and medicine: a historical perspective," *Lancet*, vol. 379, pp. 1517–1524, 2012.

[2] M. Antico, F. Sasazawa, L. Wu, A. Jaiprakash, J. Roberts, R. Crawford, et al. "Ultrasound guidance in minimally invasive robotic procedures," *Med. Image Anal.*, vol. 54, pp. 149–167, 2019.

[3] L. Magalhães, S. R. P. Martins, and R. Nogué, "The role of point-of-care ultrasound in the diagnosis and management of necrotizing soft tissue infections," *Ultrasound J.*, vol. 12, no. 1, pp. 10–15, 2020.

[4] N. Salem, H. Malik, and A. Shams, "Medical image enhancement based on histogram algorithms," *Procedia Comput. Sci.*, vol. 163, pp. 300–311, 2019.

[5] L. G. and A. Jouan, "Speckle filtering of SAR images – A comparative study between complex-wavelet-based and standard filters," *SPIE Prococess*, vol. 3169, no. 80, 1997.

[6] S. B. B. Aiazzi and L. Alparone, "on Geoscience and Remote Sensing," *IEEE Transion*, vol. 1466, pp. 36–41, 1998.

[7] A. Bovik, "Handbook of Image and Video Processing," *Acad. Press. San Diego*, no. ISBN: 0-12-119790-5., 2000.

[8] G. Y. T. T. S. Huang and G. J. Yang, "Speech and Signal Processing," *IEEE Trans. Acoust.*, vol. 27, pp. 1–13, 1979.

[9] A. I. Nasir, "Artifact in the Image of Ultrasound," *Aust. J. Basic Appl. Sci.*, vol. 12, no. 12, pp. 131–143, 2018.

[10] J. A. H. P. C. Tay and S. T. Acton, "A wavelet thresholding method to reduce ultrasound artifacts," *Comput. Med. Imaging Graph.*, vol. 35, pp. 42–50, 2011.

[11] L. Vanitha and A. R. Venmathi, "Classification of Medical Images Using Support Vector Machine," *Int. Conf. Inf. Netw. Technol.*, vol. 4, pp. 63–67, 2011.

[12] Sudhamshu Mohan S, Mr. Harsha, and Dr. Padmaja K V, "SVM based Classifier for Noise Classification in Ultrasound B - Mode Images," *Int. J. Eng. Res.*, vol. V5, no. 08, 2016.

[13] J. Verma, M. Nath, P. Tripathi, and K. K. Saini, "Analysis and identification of kidney stone using Kth nearest neighbour (KNN) and support vector machine (SVM) classification techniques," *Pattern Recognit. Image Anal.*, vol. 27, no. 3, pp. 574–580, 2017.

[14] Z. A. et Al., "An efficient gray-level co-occurrence matrix (GLCM) based approach towards classification of skin lesion," *2019 Amity Int. Conf. Artif. Intell. (IEEE, 2019)*, 2019.

[15] B. A. S. Öztürk, "Application of feature extraction and classification methods for histopathological image using GLCM, LBP, LBGLCM, GLRLM and SFTA.," *Proc. Comput. Sci.*, vol. 132, pp. 40–46, 2018.

[16] S. Vani Kumari and K. Usha Rani, "Analysis on Various Feature Extraction Methods for Medical Image Classification," no. November, pp. 19–31, 2020.

[17] R. G. B. A. Hindi, and C. Peterson, "Artifacts in diagnostic ultrasound," *Reports Med. Imaging*, vol. 6, pp. 29–48, 2013.

[18] P. E. D. J. Huang, J. K. Triedman, N. V. Vasilyev, Y. Suematsu, and R. O. Cleveland, "Imaging artifacts of medical instruments in ultrasound-guided intervention," *J. Ultrasound Med.*, vol. 26, pp. 1303–1322, 2007.

[19] R. S. W. M. S. Taljanovic, D. M. Melville, L. R. Scalcione, L. H. Gimber, and E. J. Lorenz, "Artifacts in musculoskeletal ultrasonography," *Semin. Musculoskelet. Radiol.*, pp. 03–011, 2014.

[20] K. A. Laing FC, "The importanve of ultrasonic side lobe artifact.," *Radiology*, pp. 154–763, 1992.

[21] P. Yang, Wei Song , Xiaobing Zhao and Rui Zheng Letu Qingge "An improved Otsu threshold segmentation algorithm," vol. 22, no. 1, pp. 146–153, 2020.

[22] W. Mahani Hafizah and E. Supriyanto, "Comparative Evaluation of Ultrasound Kidney Image Enhancement Techniques," *Int. J. Comput. Appl.*, vol. 21, no. 7, pp. 15–19, 2011.

[23] C.-W.Hsu, C.-C.Chang, C.-J.Lin, and others "A practical guide to support vector classification," *Dep.Comput.Sci.Inf.Technol.Natl.Taiwan Univ*, 2003.

[24] R. M. and C.Chandrasekar, "Object recognition using SVM-KNN based on geometric moment invariant," *Int.J.Comput.Trends Technol*, vol. 1, pp. 215–220, 2011.

[25] R. S. C.Cusano, and G.Ciocca, "Image annotation using SVM," *Internet imaging V*, vol. 5304, pp. 330–338, 2003.

[26] A. K. S.Nigam, and K.Deb, "Moment invariants based object recognition for different pose and appearances in real scenes," *3013 Int. Coference Informatics ,Electronics Vis.*, pp. 1–5, 2013.

[27] J. J. Cerrolaza *et al.*, "Quantification of kidneys from 3D ultrasound in pediatric hydronephrosis," *Proc. Annu. Int. Conf. IEEE Eng. Med. Biol. Soc. EMBS*, vol. 2015-Novem, pp. 157–160, 2015.

[28] S. Candemir *et al.*, "Lung segmentation in chest radiographs using anatomical atlases with nonrigid registration," *IEEE Trans. Med. Imaging*, vol. 33, no. 2, pp. 577–590, 2014.

[29] P. T. Akkasaligar, S. Biradar, and S. Badiger, *Segmentation of Kidney Stones in Medical Ultrasound Images*, vol. 1036. Springer Singapore, 2019.

[30] D. Asamoah, E. Ofori, S. Opoku, and J. Danso, "Measuring the Performance of Image Contrast Enhancement Technique," *Int. J. Comput. Appl.*, vol. 181, no. 22, pp. 6–13, 2018.

[31] M. Antico *et al.*, "Ultrasound guidance in minimally invasive robotic procedures," *Med. Image Anal.*, vol. 54, pp. 149–167, 2019.